CS-ToF sensing by means of greedy bi-lateral fusion and near-to-optimal low-density codes

Alvaro Lopez Paredes, Miguel Heredia Conde, Otmar Loffeld
Center for Sensor Systems (ZESS), University of Siegen, Germany
Email: alvaro.lparedes@uni-siegen.de, {heredia, loffeld}@zess.uni-siegen.de

***Abstract*—In this work, we propose a sensing scheme for the reconstruction of a highly sparse 3D view by a Pulse-Based Time-of-Flight (PB-ToF) camera aiming at achieving high angular resolution at interactive rates. The construction of the sensing matrices is focused on the optimization of the coherence and the preservation of the low density which characterize Low-Density Parity-Check (LDPC) codes. We investigate the possibility of shifting the custom sequences generated at the pixel level by selecting the shifts which maximize the minimum distance between adjacent columns, as well as the use of the information from the two complementary integration channels or taps the ToF sensor consists of. The signal reconstruction algorithm, coined greedy bi-lateral fusion, firstly determines a preliminary target probability distribution, and then re-weights it by exploiting the local correlations within the pixel array by applying a bi-lateral filtering which accounts for the affinities in spatial and intensity domains. The algorithm improves the accuracy of our camera under presence of strong noise and still preserves the speed and simplicity associated to classical greedy algorithms.**

***Index Terms*—bi-lateral filtering, coherence, compressive sensing, image reconstruction, time-of-flight**

I. Introduction

Compressive Sensing (CS) [1], [2] has become of vital importance over the past few decades, especially within the computer vision and signal processing communities, in the constant effort of extracting as much meaningful information as possible without the need of handling and storing a large volume of data. Over the recent years, many sensing schemes have been proposed to efficiently scatter the domain under study and only acquire and store a small amount of not-redundant data from which information is extracted, by taking advantage of the intrinsic properties of the signals considered. However this comes at the cost of more elaborated and time-consuming reconstruction methodologies. CS exploits the sparsity and compressibility existing in many natural signals, i. e., they can be precisely represented by a reduced number of coefficients in the appropriate domain.

This research is focused on the development of a PB-ToF imaging system which exploits the fact that most of the objects that surrounds us, targets in our imaging system, are confined in narrow regions and the rest of the spatial domain is empty. In a PB-ToF system a front of light pulses is sent by a dedicated illumination system, hits an object from the scene, returns to the camera and is detected by one or some of the pixels of the sensor array. In the meantime, a custom binary sequence is generated at the pixel level. The correlation between the train of delayed light pulses and each of these sequences generates a measurement. This operation is repeated until enough measurements to successfully retrieve the signal are taken. In order to minimize the acquisitions required and to reduce the computational cost associated to the reconstruction of the signal, we explore one of the fundamentals of CS, i. e., coherence. The coherence is a measurement of the similarity between the columns of the sensing matrix and a fundamental property in most reconstruction, especially greedy, algorithms. Most greedy algorithms, such as Orthogonal Matching Pursuit (OMP) [3], share a first step in which a probability distribution is determined based on the projection of the measurement vector and its subsequent residuals on the columns of the sensing matrix. Therefore, each of these columns explains how targets at different depths contribute to the measurements. Thus, uniqueness in determining the locations of the target(s) is related to dissimilitude between columns and, therefore, to the minimization of the coherence of the sensing matrix. For the sensing matrices constructed via gradient combinatorial approach [4], we focused on optimizing the orthogonality between the columns of the custom (0,1)-binary sequences and determined an upper bound for the grid discretization which guaranteed the uniqueness of the columns. In this work, we investigate the possibility of delaying the sequences, i. e., shifting the rows of the sensing matrices, to eliminate very similar columns close to the center of the non-null elements. The main consequence is the increase of the inter-column distance, which directly translates into a reduction of the overall coherence. The impact of these variations on the reconstruction outcome will be evaluated. Also, we show that further improvement is possible if we account for the structure of the sensors. With respect to the recovery of the signal, we propose an algorithm which starts by determining a preliminary discrete probability distribution in the depth domain and then re-estimate it by exploiting the local correlations within the pixel array in the spatial and intensity domains. This will avoid the catastrophic failure which sometimes classical greedy algorithms suffer under the presence of noise.

This project has received funding from the European Union's Horizon 2020 research and innovation programme under the Marie Skłodowska-Curie grant agreement No 860370.

II. Methodology

A. ToF Sensing Scheme

The ToF camera presented in Fig. 1 is based on a rotary PB-ToF imaging system which exploits the angular motion to

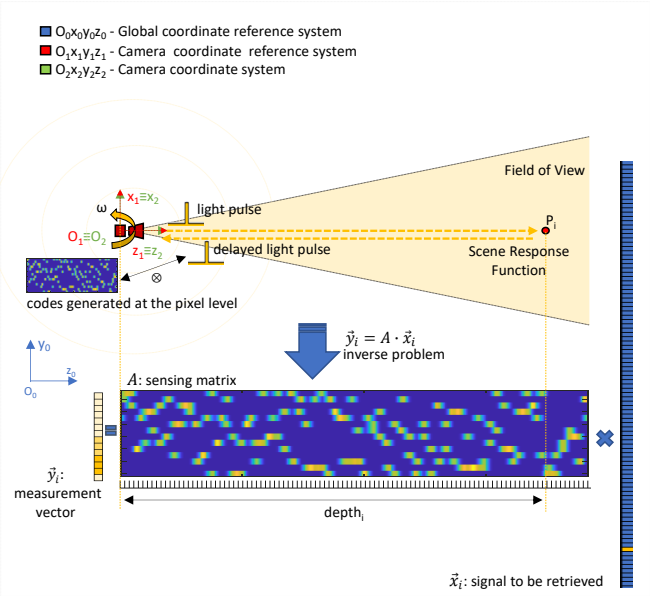

Fig. 1. ToF camera set-up and sensor model

increase the field of view (FOV), and significantly reduces the exposure time to avoid the introduction of motion artifacts into the scene. A detailed description of the ToF camera set-up and working principle is presented in [4], [5].

Any target detected by the ToF camera, P_i, is provided in spherical coordinates by the triplet $(\theta_{P_i}, \phi_{P_i}, r_{P_i})$. This triplet is defined with respect to the camera coordinate system $O_{x_2y_2z_2}$, which follows the translation and rotation of the camera and is placed at the center of the sensor plane. The emitted signal $p_{\vec{r}_i}(t)$, defined for the vector $\vec{r}_i = \vec{r}(\theta_i, \phi_i)$, interacts with the scene represented by the Scene Response Function (SRF) defined in (1), where $\delta(t)$ and $\{\Gamma_{\vec{r}_i}[k], \tau_{\vec{r}_i}[k]\}_{k=0}^{s-1}$ are the Dirac delta function and the reflectivities and time delays introduced by s return paths of light [6], [7] defined in t, respectively.

$$h_{\vec{r}_i}(t, t') = \sum_{k=0}^{s-1} \Gamma_{\vec{r}_i}[k]\delta(t - t' - \tau_{\vec{r}_i}[k]) \tag{1}$$

The SRF is a shift-invariant function and the interaction with the emitted signal can be formulated as the convolution of both signals $r_{\vec{r}_i}(t) = (p_{\vec{r}_i} * h_{\vec{r}_i})(t)$. The pixel correlates between this reflected signal against m controllable shift-invariant functions $\left[\Psi_{\vec{r}_i,j}\right]_{j=1}^{m}$ (2). Ideally, these functions are binary codes of n elements, which are further discretized in N_{steps} steps yielding n_{samples} sub-divisions.

$$y_{\vec{r}_i,j}(t) = ((p_{\vec{r}_i} * h_{\vec{r}_i}) \otimes \Psi_{\vec{r}_i,j})(t), \quad 1 \leq j \leq m \tag{2}$$

Equation (2) is translated to (3), by exploiting cyclic convolution attributes [6]. Firstly, any correlation of energy signals can be rewritten as a convolution. Thus, we can consider the overall convolution of the three signals in (2). Secondly, we can freely re-arrange the terms of the product by taking advantage of the association law and commutation properties.

$$y_{\vec{r}_i,j}(t) = ((p_{\vec{r}_i} \otimes \Psi_{\vec{r}_i,j}) * h_{\vec{r}_i})(t), \quad 1 \leq j \leq m \tag{3}$$

Hence, m measurements at $t = 0$ are originated. This yields a linear system of equations (4), where $\vec{y}_{\vec{r}_i} = [y_{\vec{r}_i,j}(t = 0)]_{j=1}^{m}$ is the measurement vector, $\boldsymbol{A}$ is the sensing matrix with $\boldsymbol{A} = \left[\left[a_j^l\right]_{j=1}^{m}\right]_{l=1}^{n_{\text{samples}}} := (p_{\vec{r}_i} \otimes \Psi_{\vec{r}_i,j})(t_i)$, and $\vec{x}_{\vec{r}_i} := [h_{\vec{r}_i}(t_i)]_{i=1}^{n_{\text{samples}}}$ is the signal being retrieved.

$$\vec{y}_{\vec{r}_i} = \boldsymbol{A} \cdot \vec{x}_{\vec{r}_i} \tag{4}$$

This system is under-determined, as $m \ll n_{\text{samples}}$, and leads to a constrained ℓ_0-minimization problem (5), i. e., to find the sparsest solution which complies with (4).

$$\hat{\vec{x}}_{\vec{r}_i} = \arg\min_{\vec{x}_{\vec{r}_i}} |\operatorname{supp}(\vec{x})|, \quad \text{subject to:} \quad \vec{y}_{\vec{r}_i} = \boldsymbol{A} \cdot \vec{x}_{\vec{r}_i} \tag{5}$$

The sensing matrices generated following the gradient-combinatorial approach [4] optimized the coherence by considering a combination without repetition of a fixed number of non-zero elements per column. Then, they prevented the coincidence of raising and falling edges between adjacent columns by arranging the columns in a specific order. However, there existed an upper limit for super-resolution. This limit was given by the maximum number of sub-divisions of each binary element which guaranteed $\mu < 1$. We now propose an extension of this algorithm by introducing an additional step at the end of the construction of the sensing matrices, which pushes these limits further, as presented in Algorithm 1. This operation can be implemented in other types of sensing matrices also yielding a positive impact on the coherence.

The algorithm introduces the possibility of horizontally shifting the different rows. The shift is a multiple of the minimum grid size in the on-grid case and may vary from the minimum grid size to the width of the initial binary element. This near-to-optimal construction scheme iteratively works per row by selecting the shift (if any) which maximizes the minimum distance between the adjacent columns, since

Algorithm 1: Near-to-optimal sensing matrix construction for *min-max* inter-column coherence

Data: $\boldsymbol{A}$, N_{steps}
Result: $\boldsymbol{A}_{\text{opt}}$
Initialize: $\boldsymbol{A}_{\text{opt}} = \boldsymbol{A}$; $k_{\max} = 0$; $d_{\max} = 0$;
for $j = 1 : m$ **do**
  for $k = 0 : N_{\text{steps}} - 1$ **do**
    $\vec{a}_{\text{opt},j} = \text{circshift}\,(\vec{a}_j, k)$;
    $d_{\min} = \min_{1 \leq l \leq n_{\text{samples}}-1} \|\vec{a}_{\text{opt}}^{l+1} - \vec{a}_{\text{opt}}^{l}\|_2$;
    if $d_{\min} \geq d_{\max}$ **then**
      $d_{\max} = d_{\min}$; $k_{\max} = k$;
    end
  end
  $\vec{a}_{\text{opt},j} = \text{circshift}\,(\vec{a}_j, k_{\max})$
end

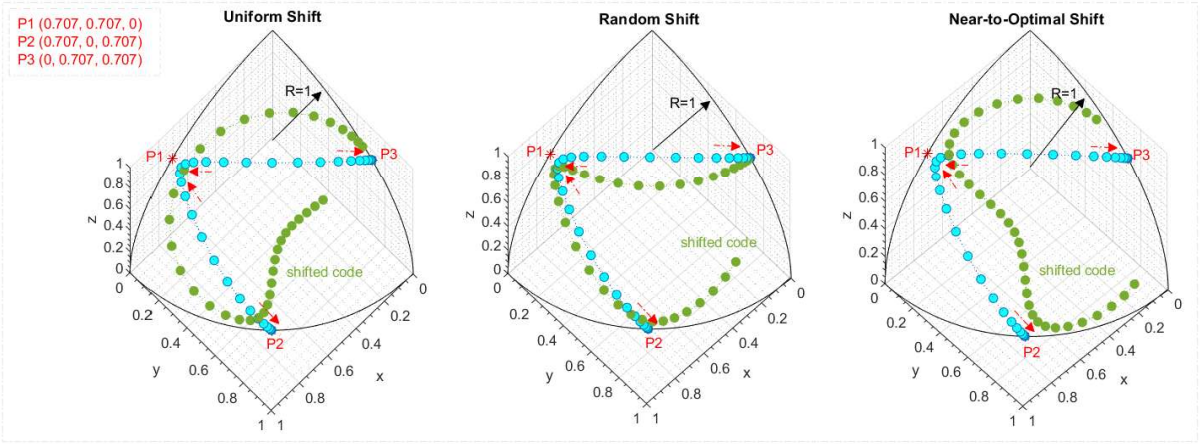

Fig. 2. Representation of normalized columns of the sensing matrices on the unit hypersphere on $\mathbb{R}^3$ for $N_{\text{steps}} = 14$, and $N_{\text{deg}} = 2$

this magnitude is inversely proportional to the coherence of the sensing matrix. The minimum distance resulting from this scheme surpasses the ones obtained in other methodologies, such as uniformly or randomly selected on-grid shifts, as shown in Fig. 3, where the minimum distances for various grid resolutions from $N_{\text{steps}} = 2$ to 20 are presented. The shifts introduced make the inter-column distance greater than zero, and, therefore, allow the resolution of inverse problems which were not initially solvable, since uniqueness of the columns of the sensing matrices ($\mu < 1$) [8] could not be ensured.

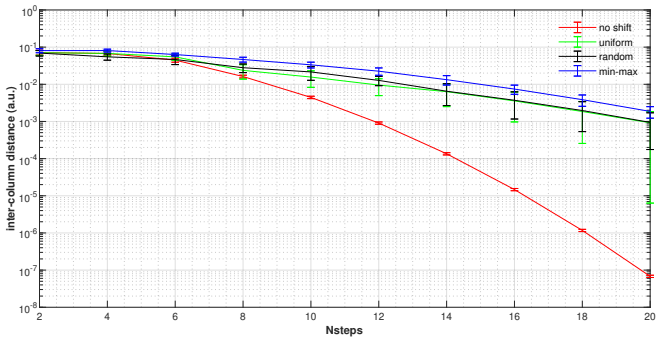

Fig. 3. Distance between adjacent columns for $m = 14$, $n = 64$, and $N_{\text{deg}} = 2$

Fig. 2 presents the distribution of n_{samples} points, representing the normalized columns of the sensing matrix A in the $\mathbb{R}^3$ space. We aim to cover as much surface of the sphere as possible by maximizing the inter-column distance. If no shift is considered, there may exist a severe concentration of samples in the vicinity of the points representing the columns of the initial binary matrix due to the pulse-shaped instrument response function (IRF), $p_{\vec{r}_i}(t)$. When the shifts are introduced, we observe two beneficial consequences: the minimum and cumulative distances between adjacent columns of the sensing matrix are significantly increased and the samples are more homogeneously distributed over the surface of the sphere. We now generalize this concept to any $\mathbb{R}^m$ space, Fig. 4 compares the original sensing matrices, the corresponding normalized Gramian matrices, and histograms of normalized scalar products between the columns of the sensing matrices from the gradient-combinatorial approach to the ones obtained when posterior shifts of the rows are implemented by considering random, uniform, and near-to-optimal max-min schemes. Since the coherence of the (0,1)-binary sensing matrices was initially optimized, the most coherent regions are confined to several cells at both sides of the main diagonal. When introducing the shifts, the width of these regions and the overall coherence are reduced.

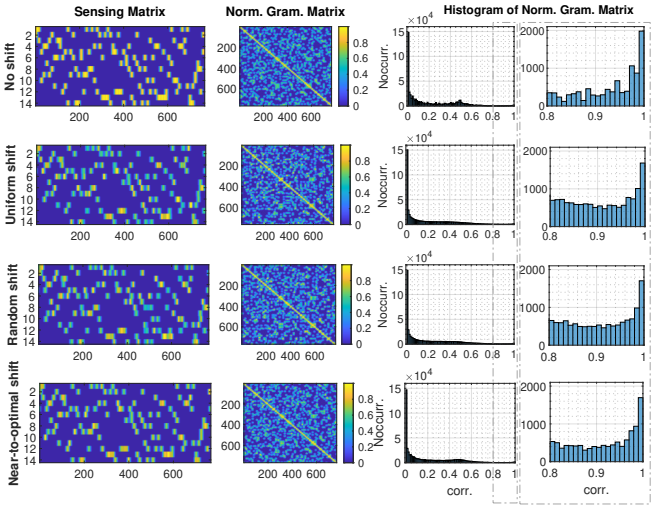

Fig. 4. Optimization of sensing matrices via custom shifting for $m = 14$, $n = 64$, $N_{\text{steps}} = 14$, and $N_{\text{deg}} = 2$

An additional step to enhance the accuracy during sensing relies on some prior knowledge of the architecture of the photo-gate PMD-based ToF sensors [7]. The sensor consists of two complementary integration channels or *taps* whose charge levels are controlled by the signal that controls the pixels, i. e., the custom codes. Supposing no background light, we propose to make use of the difference from both integration channels yielding custom sequences based on (-1,1)-binary sensing matrices and a reduction of the resulting coherence.

B. Signal Reconstruction

The ℓ_0-minimization problem (5) is generally non-convex and computationally expensive to solve. There exist three classical approaches to surpass these limitations: Basis Pursuit (BP), which relies on the relaxation from ℓ_0 to ℓ_1-minimization [9], greedy [3], and thresholding algorithms [10]. We propose a reconstruction formulation coined greedy bi-lateral fusion which starts as a classical greedy approach and, then, accounts for the local correlations within the pixel array, as described in Algorithm 2, where the weights used for the bi-lateral filtering respond to (6), being σ_k and σ_i the smoothing parameter in the spatial and intensity domains, respectively. Since the coherence optimization bounds the spread of eigenvalues of any support-restricted Gram matrix, the variation of the ℓ_2-norm of the estimate signal and the ℓ_2-norm of the residual of the measurement vector through $\boldsymbol{A}$ is bounded. Therefore, the intensity used in the bi-lateral filtering $\hat{I}^{(k,s)}$ with $1 \leq k \leq N$, being $N = n_{\text{rows}} \times n_{\text{columns}}$ and $1 \leq s \leq s_{max}$ is approximated as the residual norm $\|\vec{r}^{(k,s)}\|_2$.

$$w(i,k) = \exp\left(-\frac{\|i-k\|_2^2}{2\cdot {\sigma_k}^2} - \frac{\|\hat{I}^i - \hat{I}^k\|_2^2}{2\cdot {\sigma_i}^2}\right) \tag{6}$$

The algorithm consists of the following steps:

1) Preliminary estimation of an initial signal support, $\Gamma^{(k,s)}$ based on a discrete probability density function $\vec{g}^{(k,s)}$ which is composed of the scalar products between the residuals of the measurement vector $\vec{r}^{(k,s)}$ and the normalized columns of the sensing matrix $\vec{a}_i$ with $1 \leq i \leq n_{\text{samples}}$. The likelihood threshold, ε, is calculated using Otsu's algorithm [11]. The algorithm divides the set under study in two classes and searches for the threshold which maximizes the inter-class variance. Then, $\Gamma_1^{(k,s)}$ is estimated as the entries of $\vec{g}^{(k,s)} \geq \varepsilon$. Secondly, $\Gamma_2^{(k,s)}$ is calculated applying a hard thresholding operator $\mathcal{H}_{N_\text{r}}$ over $\vec{g}^{(k,s)}$ and preserving only the largest N_r entries. The refined support $\Gamma^{(k,s)}$ is obtained as the intersection of both subsets. The elements which do not belong to $\Gamma^{(k,s)}$ are set to zero.
2) Re-calculation of the PDFs by using bi-lateral filtering [12], [13] which takes into account the local correlations in amplitude and depth of the pixel k within the neighborhood $\Omega^{(k)}$ preliminary specified. Then, the signal support $\beta^{(k,s)}$ is re-calculated based on the re-weighted PDFs and the signal is estimated via support-restricted least squares.

With the first step we remove the low-correlated noise which may impact the bi-lateral filtering outcome by preserving the most correlated columns.With the second step we account for the information from the neighborhood by considering the local correlations in the intensity and spatial domains.

Algorithm 2: Greedy bi-lateral fusion

Data: $\boldsymbol{A}$, $\vec{y}^{(k)}$, $\Omega^{(k)}$, $s_{\max}$, ε_{tol}
Result: $\vec{x}^{(k)}$
Initialize: $s = 0$
for $k = 1 : N$ **do**
  Initialize support: $\beta^{(k,s)} = \emptyset$
  Initialize estimate: $\vec{x}^{(k,s)} = \vec{0}$
  Initialize residual: $\vec{r}^{(k,s)} = \vec{y}^{(k)}$
end
while $(\|\beta^{(k,s)}\|_0 < s_{\max})$ ***and*** $(\|\vec{r}^{(k,s)}\|_2 < \varepsilon_{\text{tol}})$ **do**
  $s = s + 1$
  for $k = 1 : N$ **do**
    $\hat{I}^{(k,s)} = \|\vec{r}^{(k,s-1)}\|_2$
    $\vec{g}^{(k,s)} = \boldsymbol{A}^{\intercal} \cdot \vec{r}^{(k,s-1)}$
    $\Gamma_1^{(k,s)} = \left\{ j | \frac{g_j^{(k,s)}}{\|\vec{a}_j\|_2} > \text{Otsu}\left(\frac{g_j^{(k,s)}}{\|\vec{a}_j\|_2}\right)\right\}$
    $\Gamma_2^{(k,s)} = \text{supp}\left(\mathcal{H}_{N_\text{r}}\left(g^{(k,s)}\right)\right)$
    $\Gamma^{(k,s)} = \Gamma_1^{(k,s)} \cap \Gamma_2^{(k,s)}$
    $\vec{g}^{(k,s)}_{\overline{\Gamma}^{(k,s)}} = 0$
  end
  for $k = 1 : N$ **do**
    $\vec{g}^{(k,s)} = \frac{\sum_{i\in\Omega^{(k)}} \vec{g}^{(i,s)} \cdot w(i,k)}{\sum_{i\in\Omega^{(k)}} w(i,k)}$
    $j_{\max} = \underset{1\leq j\leq n_{\text{samples}}}{\arg\max} \left(g_j^{(k,s)}\right)$
    Update support: $\beta^{(k,s)} = \beta^{(k,s-1)} \cup j_{\max}$
    Update estimate: $\vec{x}^{(k,s)} = \boldsymbol{A}_{\boldsymbol{\beta^{(k,s)}}}{}^{\dagger} \cdot \vec{y}^{(k)}$
    Update residual: $\vec{r}^{(k,s)} = \vec{y}^{(k)} - \boldsymbol{A}_{\boldsymbol{\beta^{(k,s)}}} \cdot \vec{x}^{(k,s)}$
  end
end

III. Numerical Results

We validate the reconstruction scheme by performing numerical simulations over Middlebury dataset 2003 depth and intensity maps [14]. An arbitrary displacement of the camera $\Delta\vec{x}_0 = [0\,\text{m}, -0.1\,\text{m}, 0.2\,\text{m}]$ is performed with respect to the initial origin of the coordinate system in the dataset and $m = 14$ measurements are taken at two angular poses $\theta_i = -15°$, and $15°$, with $\text{FOV}_\text{h} = 30°$. The maximum spatial range of the ToF camera is $r_{\max} = 10\,\text{m}$, the grid is divided in $n = 64$ elements and each of them is then discretized in N_{steps} sub-divisions. With regards to the IRF, a Gaussian filter of standard deviation $\sigma = 12\,\text{ns}$ $(3.6\,\text{m})$ [6] is applied to the custom sequences generated in the pixel to obtain a realistic representation of the measurement functions. Additive White Gaussian Noise (AWGN) with various levels of Signal-to-Noise Ratio (SNR) is used to corrupt the m measurements. The depth reconstruction error is represented by the mean value of the root mean square errors (RMSE) of each array of $N_{\text{rows}} \times N_{\text{columns}}$ signals over $N_{\text{real}} = 12$ realizations. Firstly, we evaluate the correct selection of σ_i and σ_k by performing an exhaustive search of the minimum ℓ_2-norm of the depth recovery error, as shown in Fig. 5. The optimal parameters do not depend on the grid resolution, since this is fine enough to ensure no change in the mode of failure during reconstruction. Then, we evaluate the depth recovery error with respect to on-grid GT for various grid resolutions, as shown in Fig. 6, which compares greedy bi-lateral fusion to a well-

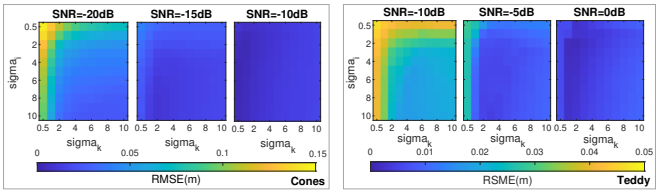

Fig. 5. Depth reconstruction error for several values of σ_i and σ_k and (-1,1)-binary shifted sequences.

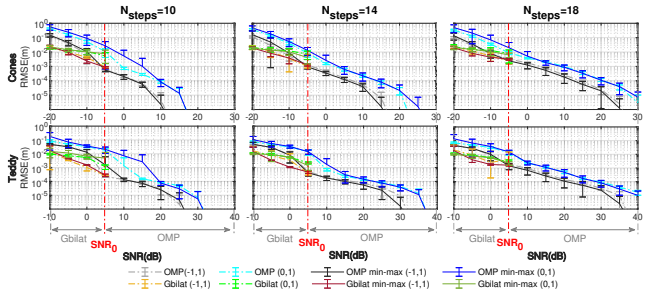

Fig. 6. Depth reconstruction error for various levels of noise and grid resolutions.

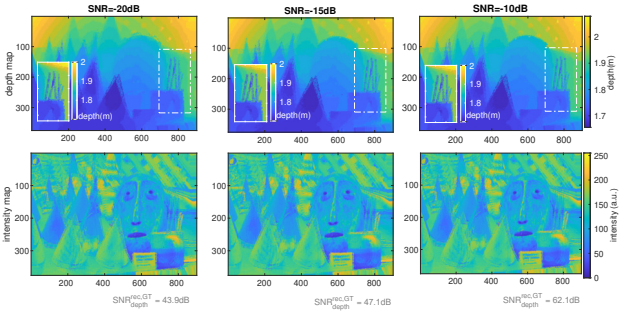

Fig. 7. Depth and intensity maps for *Cones* via greedy bi-lateral fusion with (-1,1)-binary shifted matrices.

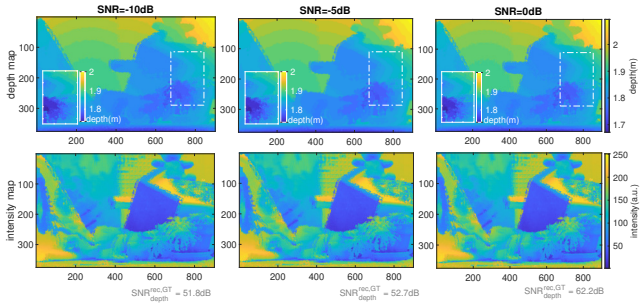

Fig. 8. Depth and intensity maps for *Teddy* via greedy bi-lateral fusion with (-1,1)-binary shifted matrices.

known greedy algorithm, such as OMP. We observe three well differentiated areas in logarithmic scale. Firstly, we observe a failure region with high reconstruction error towards the left, caused by the excessive noise in the measurements, followed by a smoother linear decrease and, finally, an abrupt reduction of the reconstruction error when exact on-grid reconstruction is reached. The improvement of accuracy is especially relevant in the first region, with a reduction of depth reconstruction error of, at least, one order of magnitude, and decreases proportionally to the noise level up to a noise threshold, SNR_0=-5 dB for *Cones* and SNR_0=5 dB for *Teddy* from which no further improvement is obtained, yielding classical OMP. Finally, we present the depth and intensity maps for various noise levels as well as the SNR of the depth maps recovered with respect to GT, $\mathrm{SNR}_{\mathrm{depth}}^{\mathrm{rec,GT}}$, in Fig. 7 and Fig. 8 for *Cones* and *Teddy*, respectively. We observe high $\mathrm{SNR}_{\mathrm{depth}}^{\mathrm{rec,GT}}$, even from very corrupted measurements, and a progressive gain in the level of detail of the retrieved depth maps as the introduced noise diminishes.

IV. Conclusions

In this paper, we thoroughly describe two algorithms to enhance the accuracy of our PB-ToF camera [4], [5]. This improvement relies on the optimization of the coherence of the sensing matrices and the use of the local correlations within the pixel array during the recovery of the signal. We show that the optimization of the sensing scheme together with the bi-lateral filtering produces a net improvement of retrieval accuracy for very noisy signals. Prospective work includes the validation of our model with real measurements on the PB-ToF camera prototype currently being developed at ZESS and the implementation of alternative reconstruction schemes.

References

[1] E. J. Candès and M. B. Wakin, "An introduction to compressive sampling," *IEEE Signal Processing Magazine*, vol. 25, no. 2, pp. 21–30, 2008.

[2] D. L. Donoho, "Compressed sensing," *IEEE Transactions on Information Theory*, vol. 52, no. 4, pp. 1289–1306, 2006.

[3] Y. C. Pati, R. Rezaiifar, and P. S. Krishnaprasad, "Orthogonal matching pursuit: recursive function approximation with applications to wavelet decomposition," in *Proceedings of 27th Asilomar Conference on Signals, Systems and Computers*, 1993, pp. 40–44 vol.1.

[4] A. Lopez Paredes, M. Heredia Conde, and O. Loffeld, "Sparsity-aware 3D ToF sensing," 2022. [Online]. Available: https://www.techrxiv.org/articles/preprint/Sparsity-aware_3D_ToF_Sensing/19161749

[5] A. Lopez Paredes, M. Heredia Conde, and O. Loffeld, "Effective very-wide-area 3D ToF sensing," in *2021 IEEE Sensors*, 2021, pp. 1–4.

[6] A. Bhandari, M. Heredia Conde, and O. Loffeld, "One-bit time-resolved imaging," *IEEE Transactions on Pattern Analysis and Machine Intelligence*, vol. 42, no. 7, pp. 1630–1641, 2020.

[7] M. Heredia Conde, *Compressive Sensing for the Photonic Mixer Device - Fundamentals, Methods and Results*. Springer, 2017.

[8] J. Tropp, "Greed is good: algorithmic results for sparse approximation," *IEEE Transactions on Information Theory*, vol. 50, no. 10, pp. 2231–2242, 2004.

[9] R. Tibshirani, "Regression shrinkage and selection via the Lasso," *Journal of the Royal Statistical Society: Series B (Methodological)*, vol. 58, pp. 267–288, 01 1996.

[10] T. Blumensath and M. E. Davies, "Iterative hard thresholding for compressed sensing," *Applied and Computational Harmonic Analysis*, vol. 27, no. 3, pp. 265–274, 2009. [Online]. Available: https://www.sciencedirect.com/science/article/pii/S1063520309000384

[11] N. Otsu, "A threshold selection method from gray-level histograms," *IEEE Transactions on Systems, Man, and Cybernetics*, vol. 9, no. 1, pp. 62–66, 1979.

[12] M. Heredia Conde, B. Zhang, K. Kagawa, and O. Loffeld, "Low-light image enhancement for multiaperture and multitap systems," *IEEE Photonics Journal*, vol. 8, pp. 1–1, 04 2016.

[13] C. Tomasi and R. Manduchi, "Bilateral filtering for gray and color images," in *Sixth International Conference on Computer Vision (IEEE Cat. No.98CH36271)*, 1998, pp. 839–846.

[14] D. Scharstein and R. Szeliski, "High-accuracy stereo depth maps using structured light," in *2003 IEEE Computer Society Conference on Computer Vision and Pattern Recognition, 2003. Proceedings.*, vol. 1, 2003, pp. I–I.